RESEARCH PAPER

The stress–strain behaviour and critical state parameters of an unsaturated granular fill material under different suctions

Kai Liu[1] · Jian-Hua Yin[1] · Wen-Bo Chen[1] · Wei-Qiang Feng[2] · Chao Zhou[1]

Abstract

In mountainous western China, a large number of granular materials are used as construction materials in high-fill embankments. These granular fill materials in the embankments are typically unsaturated owing to the arid and semi-arid climates in this area. However, previous studies on unsaturated soils primarily focus on fine-grained soils. In this study, a series of triaxial tests were performed to determine the critical state parameters of a granular fill material in q–$\bar{p}$, v–ln $\bar{p}$, and v_w–ln $\bar{p}$ planes. An upgraded double-cell triaxial system (DCTS) was used in net confining pressures ranging from 0 to 450 kPa and matric suctions ranging from 0 to 160 kPa. This study demonstrates the good performance of the upgraded DCTS in unsaturated soil testing. Experimental results show that the critical state lines are almost parallel to those of saturated soil in the q–$\bar{p}$ plane, suggesting that the friction angle is independent of suction. The total cohesion and hence the shear strength increase with suction. In the v–ln $\bar{p}$ plane, both the intercept and slope of the critical state line increase with suction. Finally, it is observed that the intercept and slope decrease with increasing suction in the v_w–ln $\bar{p}$ plane.

Keywords Critical state · High-fill embankment · Stress–strain · Suction · Unsaturated soil · Water retention curve

1 Introduction

Infrastructure constructions typically involve high-fill embankments, especially in mountainous western China. The maximum height of high-fill embankments in Jiuzhai

Wei-Qiang Feng: Formerly affiliated at "Department of Civil and Environmental Engineering, The Hong Kong Polytechnic University, Hong Kong, China.

✉ Jian-Hua Yin
cejhyin@polyu.edu.hk

Kai Liu
kevin-kai.liu@connect.polyu.hk

Wen-Bo Chen
geocwb@gmail.com

Wei-Qiang Feng
fengweiqiang2015@gmail.com

Chao Zhou
c.zhou@polyu.edu.hk

[1] Department of Civil and Environmental Engineering, The Hong Kong Polytechnic University, Hong Kong, China

[2] Department of Ocean Sciences and Engineering, The Southern University of Science and Technology, Shenzhen, China

Huanglong Airport exceeds 104 m [26]. These projects in the mountainous area require a large number of fill materials to be excavated from nearby areas and compacted in valleys. The fill materials from natural terrains are typically granular and heterogeneous soils [14, 40, 60]. These soils typically comprise a mixture of coarse (gravels) and fine particles (clays and silts). Extensive studies have been performed to investigate the behaviour of granular soils, including microporosity [17, 24, 65], hydraulic conductivity [34, 38], compression behaviour [10, 39], particle breakage [30, 62], small strain behaviour [37], numerical simulation [58], and saturated shear strength [12, 35, 57, 66]. Guo and Cui studied the pore structure of soils in the western mountainous area of China using scanning electron microscopy [17]. Yan et al. used the discrete element methods to simulate the granular materials in a landslide in the western mountainous area of China [58]. However, the behaviours of these granular and heterogeneous soils are still unclear owing to their variability and complexity [33, 36, 60].

Most of the mountainous regions of Western China are arid and semi-arid areas, which yield the unsaturated feature of fill materials. The use of these fill materials in high-fill embankments necessitates the investigation of the

unsaturated feature. This investigation requires a rational framework of the unsaturated soils to be established. Critical state frameworks for unsaturated soils have been proposed and developed in the last three decades [1, 23, 46, 56, 59, 69, 70]. The critical state frameworks for unsaturated soils comprise several important concepts, such as shear strength, yielding, and critical state. These concepts are based on reliable experimental results on unsaturated soils. Extensive studies have been performed on unsaturated soil experiments since the last decades, where time-dependent compression [9], cyclic [50, 51, 71], and various-coarse-content behaviours [52, 67], among others, have been investigated. However, most current studies on unsaturated soils focus on fine-grained soils, owing to the relative homogenisation and economic efficiency of small-sized specimens [1, 56, 64]. Few researchers have investigated the behaviour of coarse granular soils in unsaturated conditions. For the establishment of the framework of unsaturated coarse granular soils, experimental data are still scarce owing to the complex, expensive, and time-consuming tests involved [48]. Zhao and Zhang [67] studied the effect of coarse contents on the behaviour of unsaturated coarse granular soils under low net confining pressures (5–25 kPa). Nevertheless, in high-fill embankments in mountainous areas, a deep soil layer still exists in an unsaturated condition. Therefore, coarse granular soils under relatively higher confining pressures (450 kPa) must be studied. The shearing behaviour, volumetric behaviour, and critical state characteristics of coarse granular soils in unsaturated conditions are still not well understood [16].

This paper presents the experimental results of triaxial tests on an unsaturated fill material sampled from the new expansion of Chongqing Jiangbei International Airport. This study highlights the successful applicability of a new upgraded double-cell triaxial system (DCTS) for unsaturated soil testing. The stress–strain behaviour and critical state parameters of the unsaturated granular fill are emphasised. Two widely used frameworks were used to interpret the experimental results. One of them is the framework proposed by Wheeler and Sivakumar [56], which is dependent on suction. The other framework, proposed by Toll [46] and Toll and Ong [47], is based on degree of saturation.

2 Soil properties and specimen preparation

2.1 Soil properties

The soil utilised in this study was retrieved from the fill material of an embankment in the new Chongqing airport. This soil was originally weathered from Jurassic sandy mudstone and sandstone. Wet sieving and hydrometer tests
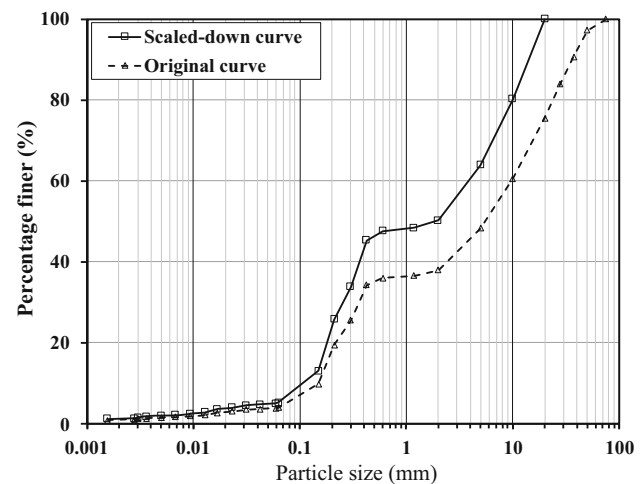

Fig. 1 Particle size distributions of the granular fill material

based the procedures in BS1377 [6] were performed to determine the particle size distribution of the soil. Figure 1 presents the particle size distribution (PSD) curves of the soil. Particles larger than 20 mm were removed to obtain a scaled-down curve [6], and the coefficient of curvature and coefficient of uniformity were calculated as 0.138 and 35.47, respectively [9, 25]. The result of the standard Proctor compaction test on the fill indicated a maximum dry density (MDD) of 2.12 Mg/m³ and optimum moisture content (OMC) of 5.7%. The studied soil can be classified as poorly graded gravel with sand (Unified Soil Classification System, USCS, ASTM D 2487) [4]. The basic soil properties are summarised in Table 1.

The filter paper method (FPM) was used to measure the matric suction, which is the pressure difference between pore-air pressure, u_a, and pore-water pressure, u_w (ASTM D 5298) [3]. The preliminary experimental results and discussions regarding the FPM can be referred to Liu et al. [25]. In addition, a pressure plate test was conducted to obtain the water retention curve (WRC) of the granular fill on a novel multipurpose testing apparatus developed in the soil mechanics laboratory of Hong Kong Polytechnic University (ASTM D 6836) [2]. The WRC of the granular fill obtained from different methods is shown in Fig. 2. The matric suction values obtained by different methods are generally consistent. The matric suction values below

Table 1 Basic soil properties of the soil

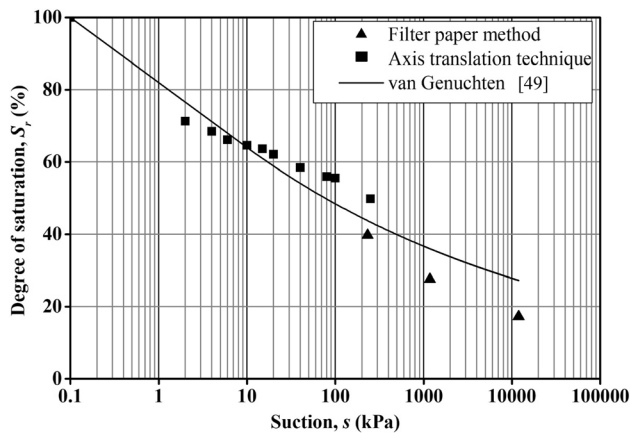| Soil property	Value
Specific gravity, G_s	2.73
Maximum dry density, $\rho_{d(max)}$ (Mg/m³)	2.12
Optimum moisture content, w_{opt} (%)	5.7
Coefficient of curvature, C_c	0.138
Coefficient of uniformity, C_u	35.47

Fig. 2 WRC of the granular fill material

Table 2 Summary of values of parameters in the van Genuchten model [49] by the best-fitting test data

a	n	m	R^2
4.1	6.308	0.02	0.96

100 kPa obtained from the FPM were not included in the plot owing to the difficulty in obtaining accurate measurements of total and matric suction using the FPM [43]. The van Genuchten model [49] expressed as Eq. (3) in "Appendix" was used to fit the experimental data (Fig. 2). Table 2 presents the best-fit model parameter values and R^2 value for the granular fill.

2.2 Soil specimen preparation

The soil specimens were prepared as follows. First, oven-dried natural soil was sieved into eight portions based on particle size: < 0.063, 0.063–0.15, 0.15–0.212, 0.212–0.3, 0.3–2, 2–5, 5–10, and 10–20 mm (Fig. 3). The granular fill samples were inhomogeneous. The soil specimens were not uniform if the particles were not separated in different particle size portions. Next, the mass of soil for each particle portion was calculated according to the scaled-down PSD curve (Fig. 1). Then, the eight portions with calculated mass were mixed uniformly. Next, the mass of water was calculated based on the targeted soil dry density and optimum moisture content. Subsequently, the mixed soil sample was mixed evenly with water with calculated mass. Next, the wet soil mixture was sealed in a plastic bag and placed in a chamber, where the soil mixture was maintained at constant temperature and humidity for at least 24 h. Finally, the soil was compacted using a rotary hammer and a steel mould in five 40-mm layers to produce a specimen of diameter 100 mm and height 200 mm. The surface of each layer was scratched to obtain an appropriate bonding with the subsequent soil layer. Each layer reached the same dry density of 1.87 Mg/m³ (88% of MDD) and moisture

content of 5.75%. Upon the completion of compaction, the mass of the specimen was recorded.

## 3 Test apparatus, test programme, and test procedure

3.1 Upgraded double cell

An upgraded suction-controlled DCTS, as shown in Figs. 4 and 5b, was first used in a series of systematically designed unsaturated triaxial tests to measure the volume changes of soil specimens [8, 15, 25, 61]. The upgraded double cell in the system could overcome two main limitations of conventional triaxial systems: the large deformation of the cell and possible water leakage in the inner cell. The long period of an unsaturated triaxial test can result in large errors of system deformation. In the conventional triaxial systems, a single cell is usually used. The pressure of de-aired water in the single cell is different from the atmospheric pressure outside of the single cell. The deformation of the cell increases with the increasing cell pressure. As shown in the double-cell triaxial system in Fig. 4, the inner cell is totally enclosed within the outer cell. De-aired water is filled in both the inner cell and the outer cell. The same magnitude of water pressure was applied in both outside and inside the inner cell. Therefore, both the wall and top cap of the inner cell have negligible deformation [61]. Errors caused by the deformation of inner cell can be avoided accordingly. In the long-period triaxial tests on unsaturated soil, especially in a cell-fluid-measurement cell, the leakage can cause large errors in volume change measurements. These possible errors can be avoided by the upgraded double cell because of a zero hydraulic gradient along the piston on the inner cell cap. Moreover, bladder air/water cylinders were used to deliver pressurised de-aired water to the double cells. The space between the inner cell and specimen was sufficient for the installation of on-sample strain transducers.
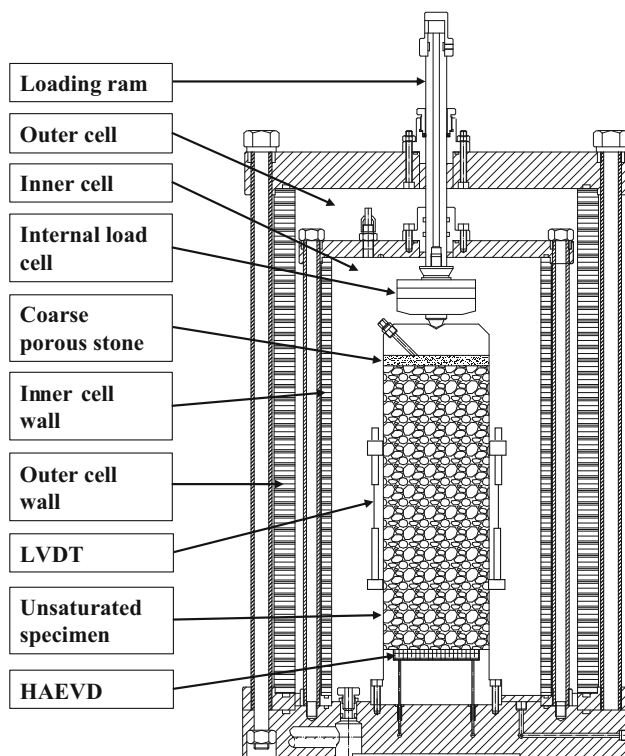
3.2 Test apparatuses

As shown in Fig. 5a, a stress-path triaxial system (SPTS) (manufactured by VJ Tech Limited, UK) was set up in the soil mechanics laboratory of the Hong Kong Polytechnic University to perform saturated consolidated drained and consolidated undrained triaxial tests. Suction-controlled consolidated drained tests were performed using a modified DCTS to study the volumetric and shear strength behaviours of an unsaturated compacted granular fill. As shown in Fig. 5b, a modified DCTS was manufactured and set up in the soil mechanics laboratory of the Hong Kong Polytechnic University.

The control of matric suction and the independent measurement of water content as well as volume changes
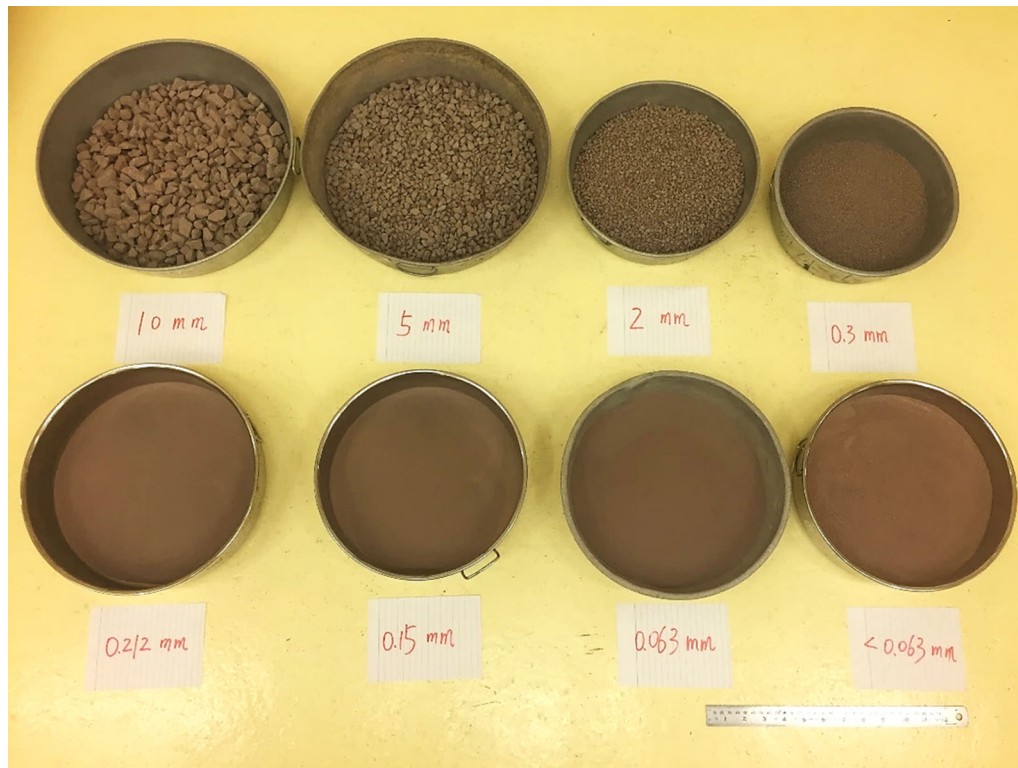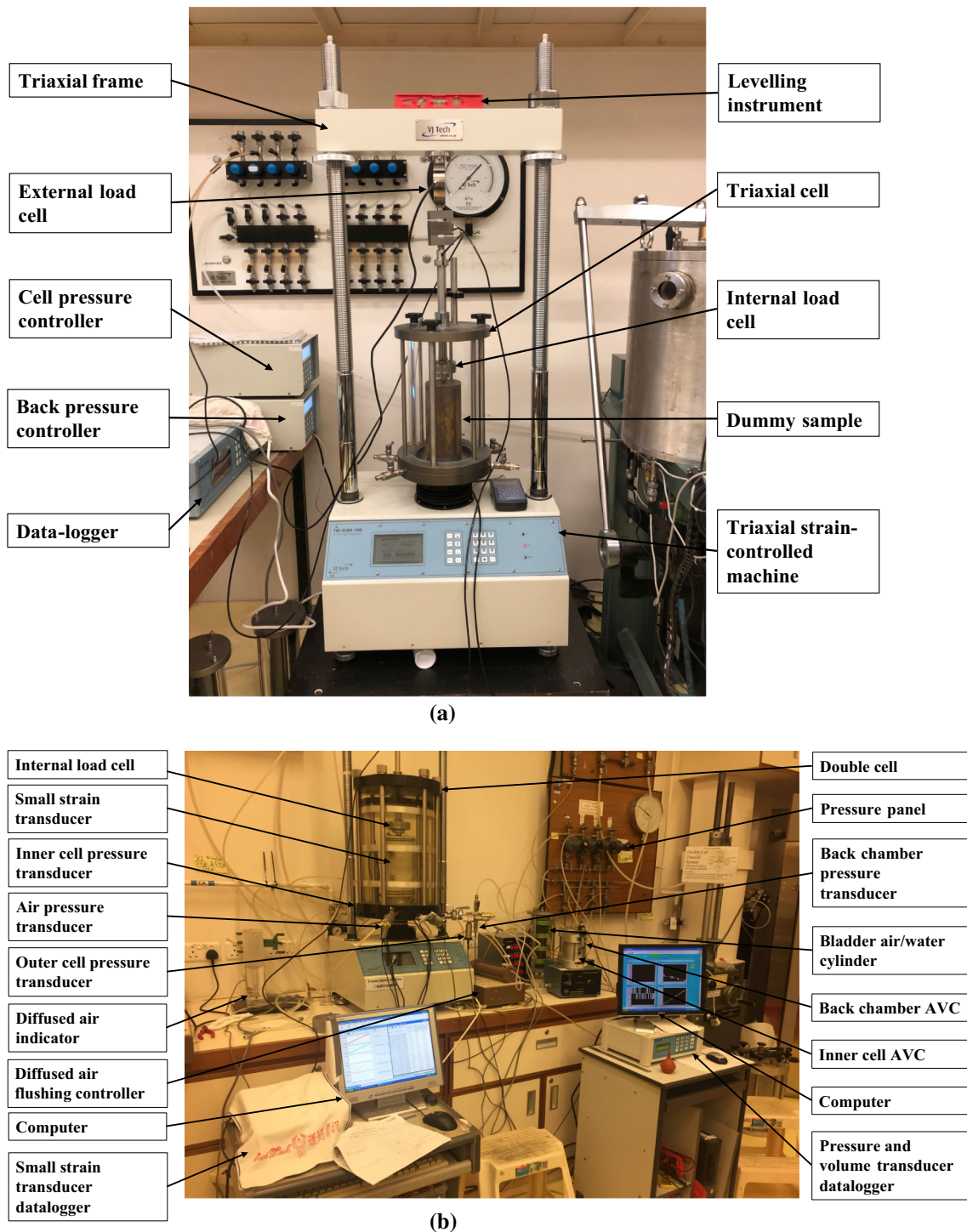
Fig. 3 Photograph of particles with different sizes preparing for soil specimens

Fig. 4 The schematic diagram of a double-cell used in triaxial tests on unsaturated soil specimens

are two main requirements for apparatuses used for unsaturated soil testing. Matric suction was controlled by the axis translation technique introduced by Hilf [19]. The axis translation technique requires the maintenance of matric suction using a high air entry value disc (HAEVD) screwed on the cell pedestal [25]. The HAEVD allowed both u_a and u_w to be controlled; therefore, the matric suction of the specimen was controlled. Two types of HAEVDs (3 and 5 bar) were used to control the matric suction. As shown in Fig. 4, a coarse porous stone was placed on the top of a soil specimen that was placed on a custom-built pedestal with a HAEVD. The air pressure and water pressure can be applied to the top of the specimen through the coarse porous stone and water chamber beneath the HAEVD, respectively. One end of the water chamber was connected to an automatic volume change (AVC) device (model type: 28-WF4410, Wykeham Farrance Engineering, Slough, Berkshire, UK) and the other end to a diffused air indicator (DAI) (model type: DAF 200 M, Geotechnical Consulting and Testing System, LLC). The AVC device and DAI were used to continuously monitor the water content change of specimen and the volume of diffused air accumulated in the water chamber. An upgraded double cell, as presented in Fig. 4, was used for the measurement of volume changes of soil specimens. One internal and one external load cells were used to determine the deviatoric stress of the specimen. Four

(a)

Internal load cell	Double cell
Small strain transducer	Pressure panel
Inner cell pressure transducer	Back chamber pressure transducer
Air pressure transducer	Bladder air/water cylinder
Outer cell pressure transducer	Back chamber AVC
Diffused air indicator	Inner cell AVC
Diffused air flushing controller	Computer
Computer	Pressure and volume transducer datalogger
Small strain transducer datalogger	

(b)

Fig. 5 Photographs of triaxial systems: **a** SPTS for triaxial tests on saturated soil specimens and **b** DCTS for triaxial tests on unsaturated soil specimens

pressure transducers were installed to measure the inner cell, outer cell, air, and water chamber pressures, respectively. A linear variable differential transformer (LVDT) was used to monitor the vertical displacement. Two types of data loggers (model types: MPX 3000 and MINISCANNER, VJ Tech Limited, UK) were used to log the data from the well calibrated measuring components, including the AVCs, DAI, LVDTs, pressure transducers, and load cells.

3.3 Test programme

A series of suction-controlled consolidated drained triaxial tests were performed to study the volumetric and shear strength behaviour of an unsaturated compacted granular fill. Additionally, a series of consolidated drained and consolidated undrained triaxial tests in saturated conditions were conducted to study the soil behaviour of specimens in a null-suction condition. The stress paths of the tests are shown in Fig. 6. The applied matric suctions ranged from 0 to 160 kPa, and the applied net confining pressures ranged from 0 to 450 kPa based on the laboratory conditions and previous studies [29, 56, 63, 68]. The net confining pressure, σ_{3c}'', is defined as the pressure difference between confining pressure, σ_{3c}, and pore-air pressure, u_a. The initial state for the unsaturated soil specimens was at point 8. The initial suction for the specimens was in the range of 20 to 40 kPa. The initial net stress for specimens was zero. As shown in Table 3, in specimen ID, the first two letters CD mean consolidated drained triaxial test, and the first number directly after the letters represents the applied matric suction, while the second number after the dash represents the applied effective confining pressure, σ_{3c}' or net confining pressure, σ_{3c}''. The effective confining pressure, σ_{3c}', is defined as the pressure difference between confining pressure, σ_{3c}, and pore-water pressure, u_w. For example, specimen ID CD40-150 means that the matric suction and net confining pressure of a specimen before shearing are 40 and 150 kPa, respectively.
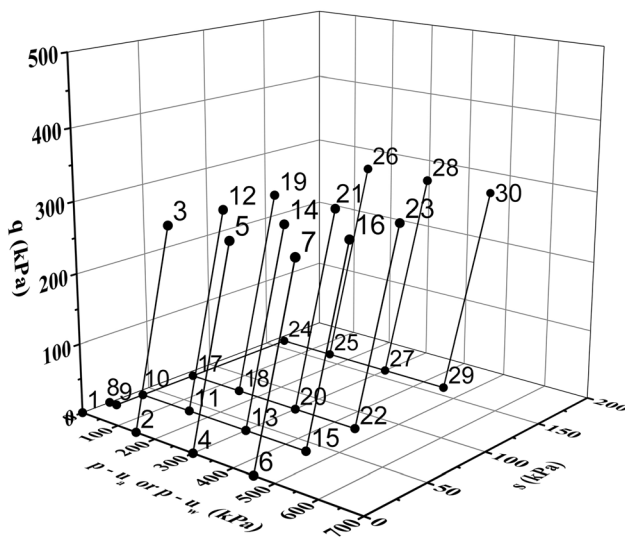
3.4 Test procedures

The test procedures of the consolidated drained and consolidated undrained triaxial tests in saturated conditions can be referred to BS 1377 [6] and Head [18].

The suction-controlled consolidated triaxial test comprises three stages, i.e. suction equalisation, isotropic compression, and constant-suction shearing. Prior to each test, several preparation procedures were performed, including the saturation of the HAEVD, leakage verification of the HAEVD, and air expulsion in the drainage lines of the inner cell and water chamber.

In the suction equalisation stage, to obtain the desired matric suction, the air pressure and water back pressure were applied to the specimen (see terminated points 10, 17, and 24 in Fig. 6). During the entire equilibration process, the total volume change and water volume change of the specimen were recorded. A net confining pressure of 20 kPa and a water back pressure of 50 kPa were maintained in the equilibration stage for each test. Several criteria in the equalisation stage have been used in the unsaturated triaxial tests. A water content change of 0.04%/day was adopted by Sivakumar [41] in unsaturated triaxial tests on compacted kaolin. Zhan [63] selected 0.02%/day of water change as a terminated criterion in a study of unsaturated expansive clay. The degree of saturation per day of less than 1% was adopted by Hossain and Yin [21] in tests on unsaturated compacted decomposed granite. Water content decrease rates of 0.2%/day and 0.04%/day were employed in unsaturated tests conducted by different research groups to measure and control suction [44]. A conservative termination criterion of the equilibration stage was set to 0.02% of water content change per day with regard to the soil property and previous studies.

After the equalisation of the desired matric suction, the constant-suction isotropic compression stages proceeded, which were sufficiently enough to enable a fully stable matric suction and drained condition to be obtained. As shown in Eq. (4), the calculation of the loading rate of consolidation was referred to a method introduced by Thomas [45]. Although the equation was used for saturated soils, the loading rate may be conservative because a lower excessive pore-water pressure was generated in unsaturated soil rather than in saturated soil under the same consolidation pressure [11, 41, 63]. The results of an oedometer test performed by Chen et al. [9] were reanalysed to obtain the coefficient of consolidation of the soil. The calculated loading rate of ramped consolidation for the granular fill was approximately 60 kPa/h. Upon the application of each net confining pressure, the specimen was left for at least 24 h to attain the full dissipation of excessive pore-water pressure in the specimen [56, 63].

Fig. 6 Stress paths of a series of triaxial tests

Table 3 Test stress paths and values of parameters for specimens at critical state

Specimen ID	Stress path (Fig. 6)	q (kPa)	$\bar{p}$ (kPa)	w (%)	S_r (%)
CD0-150	1-2-3	437.1	295.7	14.1	100
CD0-300	1-4-5	851.7	583.9	12.7	100
CD0-450	1-6-7	1228.4	859.5	11.9	100
CU0-50	–	26.9	12.2	16.3	100
CU0-100	–	55.9	32.9	15.3	100
CU0-200	–	108.2	70.9	14.5	100
CD40-150	8-9-10-11-12	389.4	279.8	7.4	50
CD40-300	8-9-10-13-14	888.7	596.2	6.3	48
CD40-450	8-9-10-15-16	1273.4	874.5	7.3	57
CD80-150	8-9-17-18-19	498.7	316.2	6.9	45
CD80-300	8-9-17-20-21	927.4	609.1	7.3	58
CD80-450	8-9-17-22-23	1328.6	892.9	6.5	59
CD160-150	8-9-24-25-26	473.4	307.8	6.6	44
CD160-300	8-9-24-27-28	980.5	626.8	5.2	40
CD160-450	8-9-24-29-30	1342.3	897.4	7.4	–

After the isotropic compression stage, the specimen was sheared in a drained condition. The net confining pressure and matric suction were applied to the specimens, and axial loads at a constant strain rate were applied to compress the specimens. Satija and Gulhati [31] used 1.3×10^{-4}%/s in consolidated drained triaxial tests on unsaturated Dhanauri clay. A strain rate of 1.7×10^{-5}%/s was employed by Ho and Fredlund [20] in the study of undisturbed decomposed granite and rhyolite. The constant strain rate in the consolidated drained triaxial tests ranged from 1.7×10^{-5} to 1.3×10^{-4}%/s. The studied soil was gravel with sand which had a high value of permeability. Therefore, a conservative constant strain rate of 3.33×10^{-5}%/s or 0.004 mm/min was adopted in this study to maintain a constant-suction condition in shearing.

The correction of the experimental data primarily included the specimen area, membrane strength, piston volume change, and cell volume change. The cell volume change included the 'immediate' volume change owing to a pressure increase and the 'creep' phenomenon under a constant pressure. Detailed descriptions can be referred to Head [18] and Chen et al. [8].

4 Experimental results and discussion

4.1 Fully saturated triaxial tests

The critical state is defined as the state of soil under continuous distortion when no change in stress or volume occurs. The critical state framework suggests a unique relationship between the void ratio (e) or specific volume (v, $v = 1 + e$) and the mean effective stress (p') [5, 32], as shown in Eqs. (5) to (9) in "Appendix". Figure 7a presents the state paths during shearing for the granular fill under saturated conditions. The specific volume of the specimen under low stresses is approximately 1.46. An approximate value of yield stress of 44 kPa can be obtained in accordance with the Casagrande method [7]. The start points of the shear paths tend to define the normal compression line (NCL) of the soil in the v–ln p' plane. Despite some scatter, the critical state points at the end of tests tend to define a critical state line (CSL) of the soil in the v–ln p' plane. The triaxial results show a possible curvature of CSLs in the v–ln p' plane. However, the linear relationship shown in Eq. (6) in "Appendix" was assumed owing to the simplicity and lack of conclusive evidence for a curving CSL. Therefore, it is likely that the CSL is parallel to the NCL. Figure 7b shows the stress paths in the q–p' plane for the six fully saturated triaxial tests. The critical state points at the end of each test probably define the CSL of the soil in the q–p' plane. This unique CSL can be defined by a stress ratio, M_s of 1.44.

Table 3 shows the stress path and values of parameters for saturated specimens at critical state. The final water contents for saturated specimens under undrained condition were calculated based on the measured water volume changes in specimens. The critical state parameters defined for soil in saturated conditions were used as a reference for soil in unsaturated conditions. The modified Cam–Clay parameters listed in Table 4 can be used to describe the behaviour of granular materials in a null-suction condition. The modified Cam–Clay parameters associated with the NCL can be described by $N_s = 1.58$, $\lambda_s = 0.033$, and
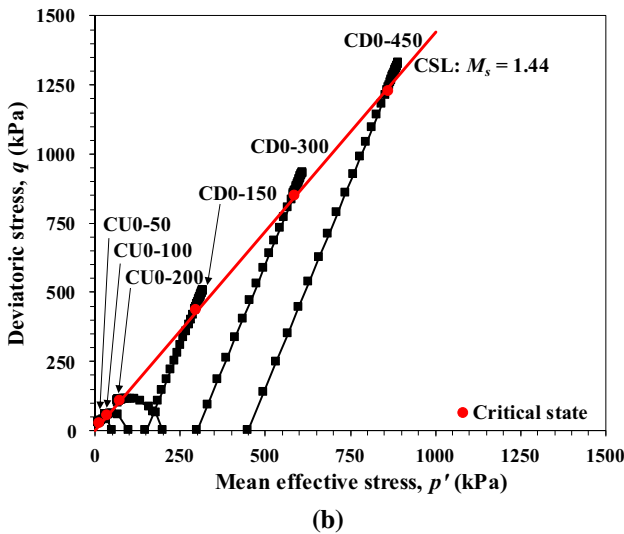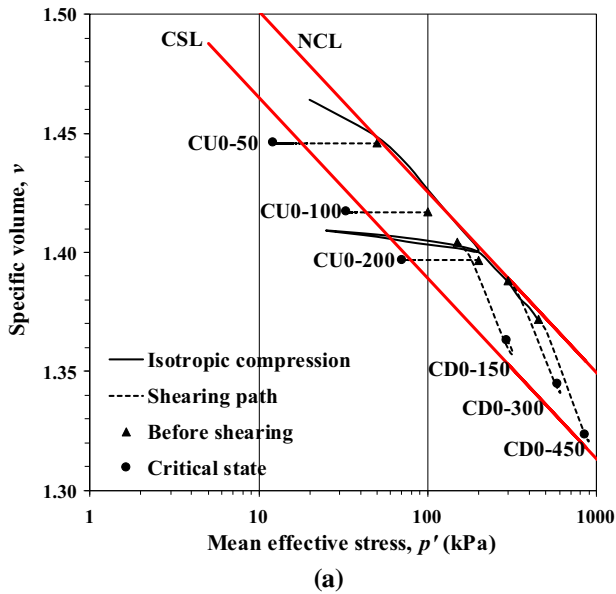
Fig. 7 Results of triaxial tests on saturated specimens: a v–ln p' plane and b q–p' plane

Table 4 Values of parameters in the modified Cam-clay model for the soil under saturated condition

N_s	λ_s	κ_s	Γ_s	M_s
1.58	0.033	0.0043	1.54	1.44

$\kappa_s = 0.0043$, while those associated with the CSL can be described by $\Gamma_s = 1.54$, $M_s = 1.44$, and $\varphi' = 35.5°$.

4.2 Stress–strain relationships

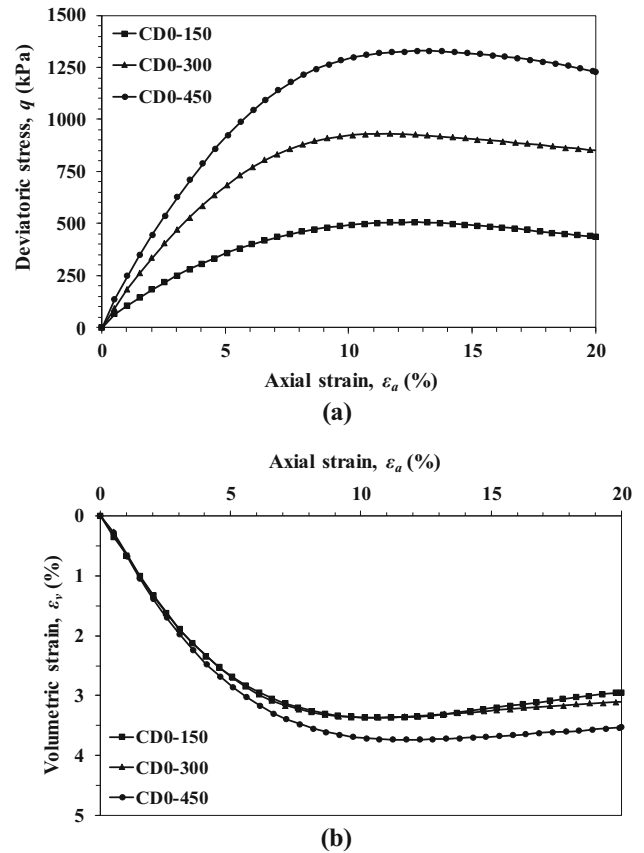Figure 8a, b presents the effect of effective confining pressure on specimens in a null-suction condition

Fig. 8 Stress–strain and volume change curves at $s = 0$ kPa and various effective confining pressures ($\sigma'_{3c} = 150$, 300, and 450 kPa): a q–ε_a plane and b ε_v–ε_a plane

($s = 0$ kPa). With an increase in the effective confining pressure, the maximum deviatoric stress and initial modulus increase. The saturated soil specimens achieved the maximum deviatoric stresses at axial strains of approximately 12%. A slight strain softening behaviour can be observed in most soil specimens. The axial strains of yielding points for the soil specimens ranged from 6 to 7%. The volumetric curves indicated an increasing trend of compressive behaviour with increasing mean effective stress. Additionally, a progressive evolution behaviour from dilation to contraction was observed with the increase in the effective confining pressure. A clear constant-volume condition could not be identified in all the specimens. Therefore, the soil specimen at an axial strain of 20% might not reach the real critical state. This phenomenon could result in a slight scatter in the CSL definition in Fig. 7a.

The typically used stress variables shown in Eqs. (1) and (2) were used to interpret the experimental results. The stress–strain and volume change curves for specimens at various net confining pressures ($\sigma''_{3c} = 150$, 300, and 450 kPa) and constant suction ($s = 160$ kPa) are shown in
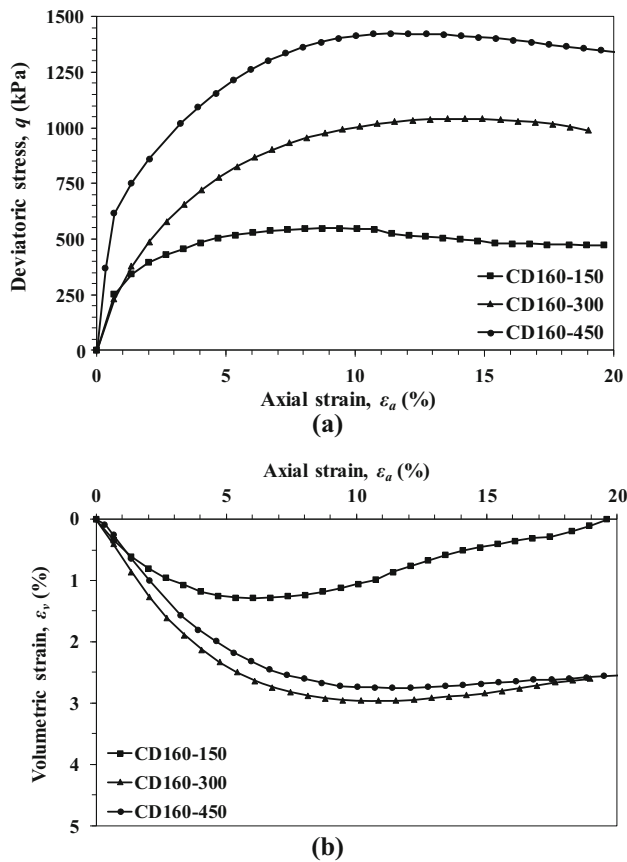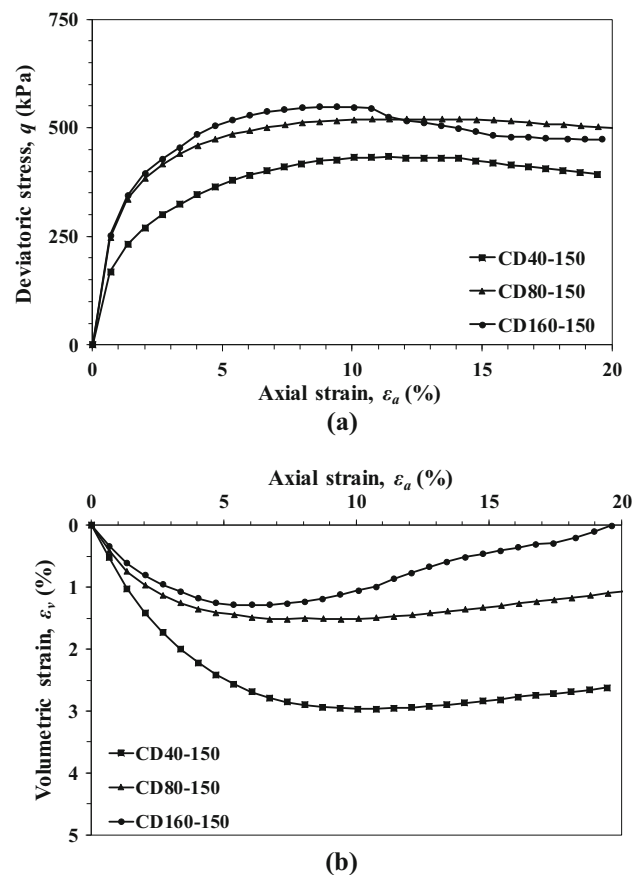
Fig. 9 Stress–strain and volume change curves at s = 160 kPa and various net confining pressures (σ''_{3c} = 150, 300, and 450 kPa): **a** q–ε_a plane and **b** ε_v–ε_a plane

Fig. 9a, b, respectively. As described previously, with increasing net confining pressure, the maximum deviatoric stress and initial modulus increased. The specimens of CD160-150 and CD160-450 reached the maximum deviatoric stresses at axial strains of approximately 10%, while that of CD160-300 reached the maximum deviatoric stress at the axial strain of approximately 14%. Additionally, they demonstrated a slight strain softening behaviour similar to those in the saturated specimens. The volumetric curves exhibited a general increasing trend of compressive behaviour with increasing net confining pressure. A possible approach between the NCL and CSL in the v–ln p' plane for unsaturated specimens under large net confining pressures may result in similar compressive behaviours for specimens under net confining pressures of 300 and 450 kPa. A progressive evolution behaviour from dilation to contraction was observed with the increase in the net confining pressure. None of the specimens demonstrated a clear constant-volume condition.

The stress–strain and volume change curves for specimens under the same net confining pressure (σ''_{3c} = 150 kPa) and various suctions (s = 40, 80, and

160 kPa) are shown in Fig. 10a, b. As shown in Fig. 10a, the maximum deviatoric stress and initial modulus increased with the matric suction. The soil specimens achieved the maximum deviatoric stresses at axial strains of approximately 9%. With the increasing suction, the strain softening behaviour was more evident. At strains larger than 9%, constant values of deviatoric stress were attained except specimen CD160-150, which possessed an apparent residual strength. The reduction of shear strength with increasing suction was also observed by some other researchers [42, 54]. This was mainly because there were less water meniscuses between aggregates at a higher suction, resulting in less water meniscus between aggregates. Hence, the contribution of suction to the inter-aggregate stress became smaller, leading to a smaller apparent cohesion. As illustrated in Fig. 10b, all the soil specimens indicated a contraction behaviour followed by a dilation behaviour during compression. Approximate trends can be observed as well, indicating that the specimens with lower suction values tend to compress more, and a greater dilatancy occurs in the higher-suction tests. These trends proved that increasing suction can facilitate

Fig. 10 Stress–strain and volume change curves at the same net confining pressure (σ''_{3c} = 150 kPa) and various suctions (s = 40, 80, and 160 kPa): **a** q–ε_a plane and **b** ε_v–ε_a plane

dilatancy [13, 23]. Generally, all the curves formed a trend regularly with the change in the matric suction. A clear constant-volume condition cannot be identified in all the specimens.

4.3 CSLs

4.3.1 CSLs in the q–$\bar{p}$ plane

The stress–strain relationships (shown in Figs. 8, 9, 10) show that the true critical states may not have been achieved owing to the continuous changes in the deviatoric stress and volumetric strain even at large strains. In triaxial shear tests on coarse granular soils, the constant-volume condition cannot be always achieved even for an axial strain of 25% [67]. This is evident in many experimental studies of on various unsaturated soils, including silt [13], gravel [46], sandy clay [47, 67], silty soil [53], and sand [67]. It is therefore difficult to obtain the true critical state for the granular materials. However, the changing rates of the deviatoric stress and volumetric strain are generally very small when the axial strain reaches 20%. Therefore, the soil state at an axial strain of 20% was assumed as the pseudo-critical state for each test.

As shown in Fig. 11a, despite some scatter in the data, the overall features are unambiguous. Based on Eq. (10) in "Appendix", linear regression was performed to evaluate the critical state parameters. The slope of the CSL, $M(s)$, in the q–$\bar{p}$ plane, appears to be independent of the matric suction and can be determined by the position of the CSL for saturated soil in the q–$\bar{p}$ plane. These results agree well with the generally accepted view that $M(s)$ is constant with suction [1, 28, 53]. Because of the decrease in deviatoric stress of specimen CD160-150 described in Sect. 4.2, this specimen was not included in the linear regression. The result for specimen CD40-150 was not included in the linear regression owing to an unknown relatively low shear stress. As shown in Fig. 12a, $\mu(s)$ increased linearly with suction. This trend is consistent with that in a previous study, where an increase in $\mu(s)$ with suction was reported [1, 27, 56]. However, the almost linear trend of $\mu(s)$ for the granular fill is not consistent with the nonlinear trend reported by Wheeler and Sivakumar [56]. To summarise, the friction angle is independent of suction and the total cohesion; hence, the shear strength increases with suction.

4.3.2 CSLs in the v–ln $\bar{p}$ plane

The state variables of the specimens at the end of tests can be plotted as shown in Fig. 11b. In the plot, the linear relationship of Eq. (11) in "Appendix" was assumed for the state variables of specimens under each suction. These linear relationships can be intuitively identified as CSLs;
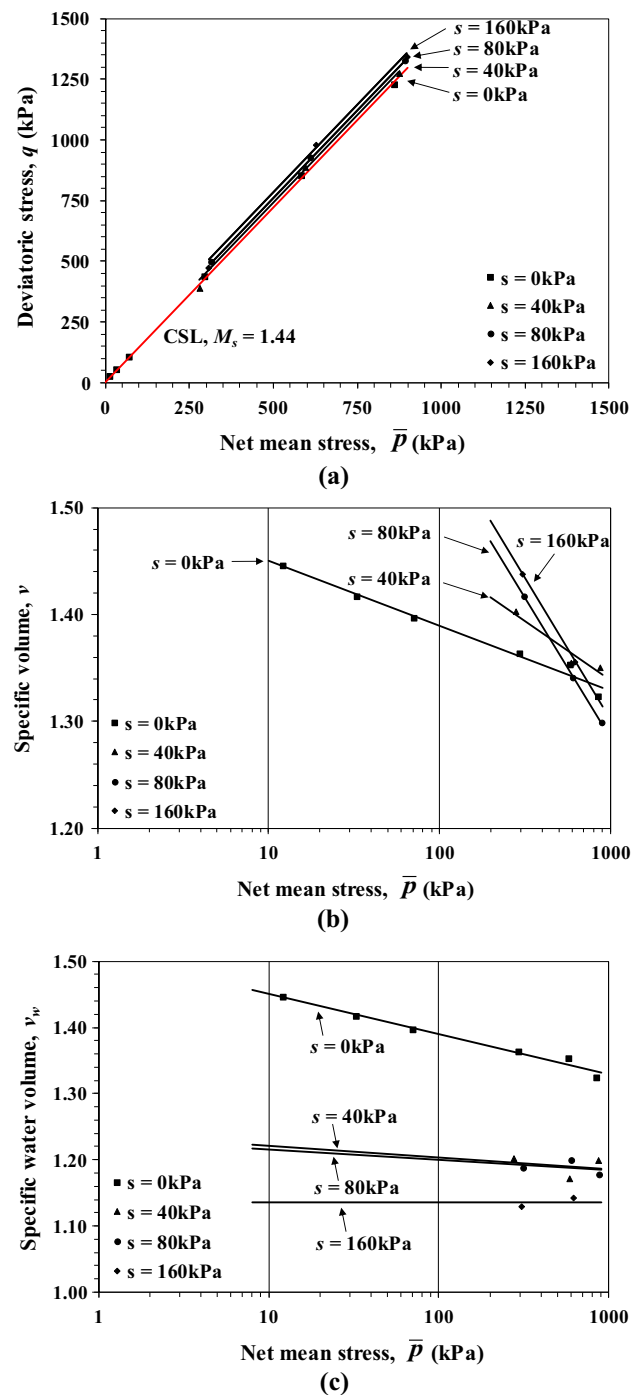
Fig. 11 Critical state conditions in different planes for the granular fill under four different suctions (s = 0, 40, 80, and 160 kPa): **a** q–$\bar{p}$ plane, **b** v–ln $\bar{p}$ plane, and **c** v_w –ln $\bar{p}$ plane

however, the results still indicated some inconsistencies in the positions of the CSLs. As shown in Figs. 9 and 10, the dilative behaviour of specimen CD160-150 is evident; therefore, the specimen may not reach the real critical state. Moreover, the result of specimen CD160-450 was not included owing to the measurement interruption of the total
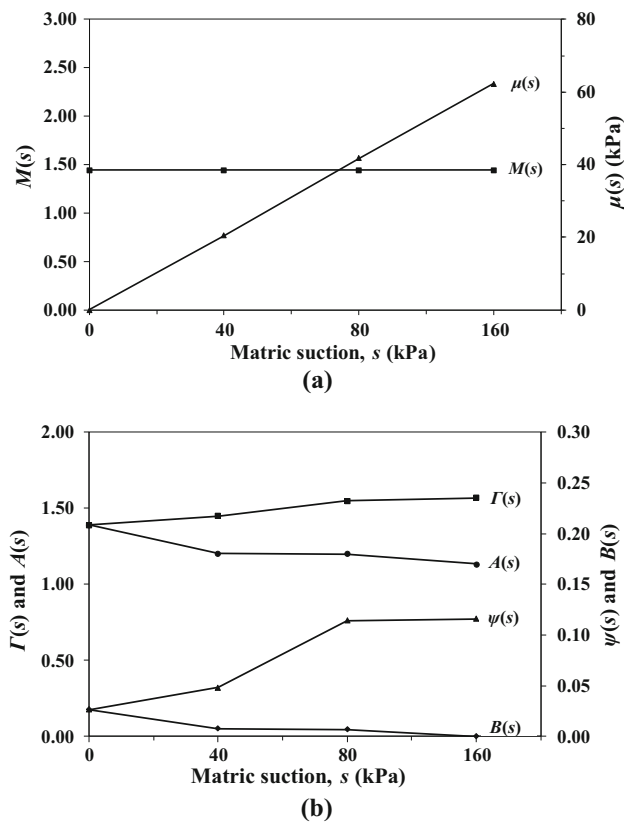
Fig. 12 a Relations of intercepts and slopes of CSLs in the q–$\bar{p}$ plane with suction and **b** relations of intercepts and slopes of CSLs in the v–$\ln \bar{p}$ plane and in the v_w–$\ln \bar{p}$ plane with suction

volume change. Figure 12b shows that both the intercept, $\Gamma(s)$ and slope, $\psi(s)$ of the CSL increase with suction. These results agree well with those of previous studies; in that, the slope of the CSL is dependent on suction [27, 56]. Nevertheless, these findings differ from those of Wang et al. [53], who argued that the slope of a CSL is equal to that of a saturated CSL and is independent of suction. In addition, Wheeler and Sivakumar [55] and Maatouk et al. [27] observed a convergent behaviour in unsaturated compacted kaolin and silty soil, respectively. However, it is difficult to identify a clear convergent point in the v–$\ln \bar{p}$ plane in this study. Despite some scatter, a possible convergent range can be identified, corresponding to a net mean stress ranging from 650 to 1000 kPa.

4.3.3 CSLs in the v_w–$\ln \bar{p}$ plane

In the v_w–$\ln \bar{p}$ plane, the linear relationship shown in Eq. (12) in "Appendix" was assumed. Variations in the CSL and corresponding critical state parameters are shown in Figs. 11c and 12b, respectively. Despite some scatter, the data support the possible existence of CSLs. The slope $B(s)$ in the v_w–$\ln \bar{p}$ plane based on Eq. (12) is equivalent to $\psi(s)$ in the v–$\ln \bar{p}$ plane in the null-suction condition. Both

the slope $B(s)$ and intercept $A(s)$ decrease with increasing suction (Figs. 11c, 12b). It appears that the drainage from the specimen decreased with the increasing suction. This finding is consistent with that by Sivakumar et al. [42] for unsaturated kaolin. Meanwhile, it is noteworthy that the v_w of each specimen was still changing at the critical state. However, as presented in Fig. 11c, the lines can be generally defined based on the experimental results under each suction. This finding broadly supports the study of Wheeler and Sivakumar [56], which showed that a pseudo-critical state relationship for v_w could provide an approximate prediction of the change in v_w, even if v_w was not strictly a state variable.

4.4 Interpretation based on S_r-dependent framework for unsaturated soils

4.4.1 Critical state stress ratios

Table 3 lists the values of parameters for specimens at the critical state. Unavailable experimental results are represented with dashed marks in the table. The values of degree of saturation at the end of the unsaturated triaxial tests range from 40% to 60%. As shown in Fig. 13a, these two stress ratio parameters are analogous to the stress ratio of saturated soil, M_s, which is defined in the q–p' space (Fig. 7b). The two stress ratio parameters, M_a and M_b, shown in Eq. (13) in "Appendix", can be derived based on the stress and state variables at the end of the tests. Similar procedures suggested by Toll and Ong [47] were used to derive the two stress ratios. First, the M_a was initially assumed to be independent of S_r and equal to M_s. Therefore, M_b could be determined based on Eq. (13). The derived M_a and M_b might be inconsistent with the degree-of-saturation-dependent functions. Therefore, a similar trial-and-error method suggested by Toll and Ong [47] was adopted to adjust and determine the M_a and M_b. The S_r tended to result in the non-uniqueness of two stress ratios.

Figure 13a shows the assessment results of M_a and M_b. The general trend is clear, despite some scatter in the figure. The values of M_a and M_b range from 0.01 to 1.57. M_a and M_b tend to approach the value of $M_s = 1.44$ at a high degree of saturation. With the decrease in S_r, M_a increased gently. Contrarily, M_b decreased considerably with decreasing S_r, and reached a value of 0.01 at a degree of saturation of approximately 40%. The results were consistent with those of Toll [46] and Toll and Ong [47] for lateritic gravel and residual sandy clay, respectively. Curves associated with the functions listed in Eqs. (14) and (15) in "Appendix" were drawn using values of $S_{r1} = 100\%$, $S_{r2} = 39\%$, $\left(\frac{M_a}{M_s}\right)_{\max} = 1.05$, $k_a = 1$ for M_a, and $k_b = 2$ for M_b. The results seem to support the assumption
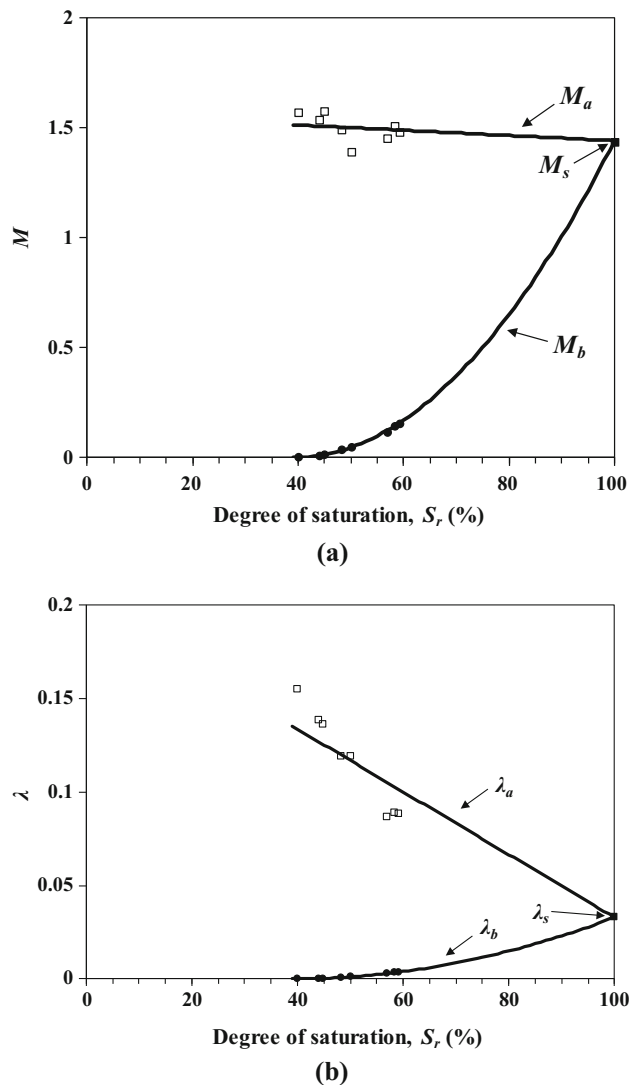
Fig. 13 Variation of critical state parameters with degree of saturation: **a** stress ratio and **b** compressibility

concluded by Jotisankasa et al. [22]; in that, it is difficult to propose relationships for specimens with degrees of saturation greater than 60%. It is necessary to conduct more experimental studies to establish relationships in this range.

4.4.2 Critical state compressibilities

As suggested by Toll [46] and Toll and Ong [47], Γ_{ab} is related to Γ_s and S_r. Similar to the case of stress ratios, λ_a and λ_b do not have unique values and are correlated with S_r. Based on Eqs. (16) and (17) in "Appendix", by the assessment of parameter values for specimens at the critical state shown in Table 3, λ_a and λ_b can be determined. Similar calculation procedures for M_a and M_b were used to determine λ_a and λ_b, respectively. In the calculation, Eqs. (18) and (19) in "Appendix" show the functions of λ_a

and λ_b, respectively, which are similar to those of M_a and M_b shown in Eqs. (14) and (15), respectively. Figure 13b shows the assessment results of λ_a and λ_b. The main trends can be identified, although some scatter is observed for the function of λ_a with experimental data. Furthermore, λ_a and λ_b tend to approach $\lambda_s = 0.033$ at a high degree of saturation. With the decrease in S_r, λ_a increased significantly. Conversely, λ_b decreased gently with the decrease in S_r and reached a value of 0.0001 at a degree of saturation of approximately 40%. The same values used for functions of stress ratios can be adopted in the functions of compressibility: $S_{r1} = 100\%$, $S_{r2} = 39\%$, $(\frac{\lambda_a}{\lambda_s})_{max} = 4.1$, $k_a = 1$ for λ_a, and $k_b = 2$ for λ_b. Figure 13b shows that the functions can provide a reasonable fit to the experimental data. These results agree well with the data reported by Toll [46] and Toll and Ong [47]. Hence, this work seems to support the findings of Toll [46] and Toll and Ong [47], who assumed that the form of the proposed functions might be applicable to a wide range of soil types.

5 Conclusions

Herein, the experimental results and interpretations of triaxial tests on an unsaturated compacted granular fill using an upgraded suction-controlled DCTS were presented. The stress–strain behaviour and critical state parameters of the unsaturated granular fill were emphasised. The experimental results of specimens in unsaturated conditions were interpreted based on two well-known frameworks: a suction-based framework developed by Wheeler and Sivakumar [56] and a degree-of-saturation-based framework proposed by Toll [46] and Toll and Ong [47]. Based on the test results and their interpretation and discussion, the following findings and conclusions were obtained:

1. The tests conducted demonstrated a successful application of an upgraded suction-controlled DCTS. It was discovered that the upgraded double cell in the system overcame two major limitations of conventional triaxial systems: large deformation of the cell and possible water leakage in the inner cell.
2. It was discovered from saturated triaxial tests that the modified Cam–Clay parameters associated with NCL could be described by $N_s = 1.58$, $\lambda_s = 0.033$, and $\kappa_s = 0.0043$. The critical state ratio M_s was 1.44, which corresponded to an effective friction angle of 35.5°.
3. It was observed from the measured stress–strain behaviour from the unsaturated triaxial tests that the maximum deviatoric stress and initial modulus increased with matric suction. With the increasing suction, the strain softening behaviour was more

evident. Specimens with lower suction values tended to compress more, and a greater dilation occurred in the higher-suction tests.

4. Based on the suction-dependent framework, the slope of the CSLs, $M(s)$ appeared to be independent of matric suction, and the intercept, $\mu(s)$ increased linearly with suction, suggesting that the friction angle was independent of suction. The total cohesion and hence the shear strength increased with suction. In the v–ln $\bar{p}$ plane, both the intercept $\Gamma(s)$ and slope $\psi(s)$ of the CSL in the v–ln $\bar{p}$ plane increased with suction. Both the slope $B(s)$ and intercept $A(s)$ in the v_w–ln $\bar{p}$ plane decreased with increasing suction.

5. The critical states were interpreted using a degree-of-saturation-dependent framework proposed by Toll [46] and Toll and Ong [47]. Two degree-of-saturation-dependent stress ratio parameters, M_a and M_b, tended to approach $M_s = 1.44$ at a high S_r. With the decrease in S_r, M_a increased gently. Contrarily, M_b decreased considerably with the decrease in S_r and reached a value of 0.01 at a degree of saturation of approximately 40%. Similarly, λ_a and λ_b did not have unique values and were correlated with S_r. The λ_a and λ_b tended to approach the value of $\lambda_s = 0.033$ at high S_r. With the decrease in S_r, λ_a increased significantly. Conversely, λ_b decreased gently with the decrease in S_r.

Appendix: Mathematical formulations used in this study

Stress variables

Two stress variables adopted are expressed as follows, including net mean stress ($\bar{p}$) and matric suction (s):

$$\bar{p} = p - u_a = \frac{\sigma_1 + \sigma_2 + \sigma_3}{3} - u_a \tag{1}$$

$$s = u_a - u_w \tag{2}$$

where σ_1, σ_2, and σ_3 are principal stresses and u_a and u_w are pore-air pressure and pore-water pressure, respectively.

WRC model

A smooth and closed-form model proposed by van Genuchten [49] was used to fit the experimental data:

$$S_r = \frac{1}{[1 + (\psi/a)^n]^m} \tag{3}$$

where S_r denotes the degree of saturation, ψ denotes soil suction, and a, n, and m denote three curve-fitting parameters.

Isotropic compression stage

An equation was proposed by Thomas [45] to describe the excess pore-water pressure produced by the ramped consolidation with increasing total stress in a saturated soil specimen. The equation was used to derive the loading rate in isotropic compression stage as follows:

$$R_L = \frac{2u_{ex}c_v}{h^2} \tag{4}$$

where R_L denotes the loading rate, h denotes drainage path length, c_v denotes coefficient of consolidation, and u_{ex} denotes excess pore-water pressure which was assumed as 2 kPa.

Critical state framework for saturated soils

The unique relationship is defined for the CSL in critical state framework. The equations for CSL proposed by Schofield and Wroth [32] are listed as follows:

$$q = M_s p' \tag{5}$$

$$v = \Gamma_s - \lambda_s \ln p' \tag{6}$$

$$M_s = \frac{6 \sin \varphi'}{3 - \sin \varphi'} \tag{7}$$

where q denotes deviatoric stress, p' denotes mean effective stress, M_s denotes slope of CSL in the q–p' plane, Γ_s denotes intercept of CSL at 1 kPa in the v–ln p' plane, λ_s denotes slope of CSL in the v–ln p' plane, and φ' denotes angle of effective friction angle.

Additionally, Eqs. (8) and (9) are used to describe the compression and swelling behaviour of soil [32]:

$$v = N_s - \lambda_s \ln p' \tag{8}$$

$$v = v_k - \kappa_s \ln p' \tag{9}$$

where N_s denotes intercept of normal compression line (NCL) at 1 kPa in the v–ln p' plane, λ_s denotes slope of NCL in the v–ln p' plane, v_κ denotes intercept of unloading/reloading curve at 1 kPa in the v–ln p' plane, and κ_s denotes slope of unloading/reloading curve in the v–ln p' plane.

Suction-based framework for unsaturated soils

Easy-to-understand linear equations for critical states proposed by Wheeler and Sivakumar [56] are listed as follows:

$$q = M(s)\bar{p} + \mu(s) \tag{10}$$

$$v = \Gamma(s) - \psi(s)\ln\left(\frac{\bar{p}}{p_{\mathrm{at}}}\right) \tag{11}$$

$$v_{\mathrm{w}} = A(s) - B(s)\ln\left(\frac{\bar{p}}{p_{\mathrm{at}}}\right) \tag{12}$$

where the parameters $M(s)$ and $\mu(s)$ are the slopes and the intercepts of critical state lines in the q–$\bar{p}$ plane, respectively. $\Gamma(s)$ and $A(s)$ are the intercepts of critical state lines at $\bar{p} = 1$ kPa in the v–$\ln\bar{p}$ and v_{w}–$\ln\bar{p}$ planes, respectively. $\psi(s)$ and $B(s)$ are slopes of critical state lines in the v–$\ln\bar{p}$ and v_{w}–$\ln\bar{p}$ planes, respectively. v_w is specific water volume ($v_{\mathrm{w}} = 1 + S_r e$), and p_{at} is the atmospheric pressure, taken as 100 kPa [56].

S_r-based framework for unsaturated soils

A degree-of-saturation-dependent framework proposed by Toll [46] and Toll and Ong [47] is listed as follows to model the critical state stress ratios for unsaturated soils:

$$q = M_{\mathrm{a}}(p - u_{\mathrm{a}}) + M_{\mathrm{b}}(u_{\mathrm{a}} - u_{\mathrm{w}}) \tag{13}$$

$$\frac{M_{\mathrm{a}}}{M_{\mathrm{s}}} = \left(\frac{M_{\mathrm{a}}}{M_{\mathrm{s}}}\right)_{\max} + \left[\left(\frac{M_{\mathrm{a}}}{M_{\mathrm{s}}}\right)_{\max} - 1\right]\left(\frac{S_r - S_{r2}}{S_{r1} - S_{r2}}\right)^{k_a} \tag{14}$$

$$\frac{M_{\mathrm{b}}}{M_{\mathrm{s}}} = \left(\frac{S_r - S_{r2}}{S_{r1} - S_{r2}}\right)^{k_b} \tag{15}$$

where M_a and M_b are the stress ratios, which can define the shear strength arising from net mean stress and matric suction, respectively. S_{r1} is the degree of saturation at full saturation (first reference state), S_{r2} is the degree of saturation at residual suction (second reference state) [48], and parameters k_a and k_b are defined to provide a degree of curvature for the function between the two reference states.

The equations of critical state compressibilities for unsaturated soils are shown as follows:

$$\Gamma_{\mathrm{ab}} = 1 + \frac{\Gamma_{\mathrm{s}} - 1}{S_{\mathrm{r}}} \tag{16}$$

$$v = \Gamma_{\mathrm{ab}} - \lambda_{\mathrm{a}}\ln(p - u_{\mathrm{a}}) - \lambda_{\mathrm{b}}\ln(u_{\mathrm{a}} - u_{\mathrm{w}}) \tag{17}$$

$$\frac{\lambda_{\mathrm{a}}}{\lambda_{\mathrm{s}}} = \left(\frac{\lambda_{\mathrm{a}}}{\lambda_{\mathrm{s}}}\right)_{\max} + \left[\left(\frac{\lambda_{\mathrm{a}}}{\lambda_{\mathrm{s}}}\right)_{\max} - 1\right]\left(\frac{S_r - S_{r2}}{S_{r1} - S_{r2}}\right)^{k_a} \tag{18}$$

$$\frac{\lambda_b}{\lambda_{\mathrm{s}}} = \left(\frac{S_r - S_{r2}}{S_{r1} - S_{r2}}\right)^{k_b} \tag{19}$$

where Γ_{ab} is a parameter related to Γ_s and S_r, λ_a and λ_b are functions of the degree of saturation and soil fabric, and

S_{r1}, S_{r2}, k_a, and k_b are the parameters similar to those used for stress ratios.

References

1. Alonso EE, Gens A, Josa A (1990) A constitutive model for partially saturated soils. Géotechnique 40(3):405–430
2. ASTM D 6836 (2002) Standard test methods for determination of the soil water characteristic curve for desorption using a hanging column, pressure extractor, chilled mirror hygrometer, and/or centrifuge. ASTM International, West Conshohocken
3. ASTM D 5298 (2010) Standard test method for measurement of soil potential (suction) using filter paper. ASTM International, West Conshohocken
4. ASTM D 2487 (2011) Standard practice for classification of soils for engineering purposes (Unified Soil Classification System). ASTM International, West Conshohocken
5. Atkinson J (2007) The mechanics of soils and foundations. CRC Press, Cambridge
6. BS 1377 (1990) Methods of test for soils for civil engineering purposes. BSI, London
7. Casagrande A (1936) The determination of the preconsolidation load and its practical influence. In: Proceedings of 1st international conference on soil mechanics and foundation engineering, Boston, Discussion D-34. Vol. 3
8. Chen WB, Yin JH, Feng WQ (2020) A new double-cell system for measuring volume change of a soil specimen under monotonic or cyclic loading. Acta Geotech 14(1):71–81
9. Chen WB, Liu K, Feng WQ, Borana L, Yin JH (2020) Influence of matric suction on nonlinear time-dependent compression behavior of a granular fill material. Acta Geotech 15:615–633
10. Chen WB, Liu K, Yin ZY, Yin JH (2019) Crushing and flooding effects on one-dimensional time-dependent behaviors of a granular soil. Int J Geomech 20(2):04019156
11. Chiu CF (2001) Behaviour of unsaturated loosely compacted weathered materials. Ph.D. Dissertation, The Hong Kong University of Science and Technology, Hong Kong, China
12. Coop MR, Lee IK (1993) The behaviour of granular soils at elevated stresses. In: Predictive soil mechanics. Proceedings of the Wroth memorial symposium, Oxford, 1992, pp 186–198
13. Cui YJ, Delage P (1996) Yielding and plastic behaviour of an unsaturated compacted silt. Géotechnique 46(2):291–311
14. Feng WQ, Li C, Yin JH et al (2019) Physical model study on the clay–sand interface without and with geotextile separator. Acta Geotech 14:2065–2081
15. Feng WQ, Yin JH, Tao XM, Tong F, Chen WB (2017) Time and strain-rate effects on viscous stress–strain behavior of plasticine material. Int J Geomech 17(5):04016115
16. Fredlund DG, Houston SL (2009) Protocol for the assessment of unsaturated soil properties in geotechnical engineering practice. Can Geotech J 46(6):694–707
17. Guo CX, Cui YF (2020) Pore structure characteristics of debris flow source material in the Wenchuan earthquake area. Eng Geol 267:105499
18. Head KH (1998) Manual of soil laboratory testing. Wiley, New York
19. Hilf JW (1956) An investigation of pore-water pressure in compacted cohesive soils. Ph.D. Dissertation, Technical Memorandum, No. 654, United State Department of the Interior Bureau of Reclamation, Design and Construction Division, Denver, Colorado, USA

20. Ho DY, Fredlund DG (1982) Increase in strength due to suction for two Hong Kong soils. In: Proceedings of the ASCE specialty conference on engineering and construction in tropical and residual soils, Hawaii, pp 263–296

21. Hossain MA, Yin JH (2010) Behavior of a compacted completely decomposed granite soil from suction controlled direct shear tests. J Geotech Geoenviron Engng ASCE 136(1):189–198

22. Jotisankasa A, Coop M, Ridley A (2009) The mechanical behaviour of an unsaturated compacted silty clay. Géotechnique 59(5):415–428

23. Li J, Yin ZY, Cui YJ, Liu K, Yin JH (2019) Hydro-mechanical modelling of unsaturated sand and clay with an explicit saturation-degree-dependent CSL. Eng Geol 260:105240

24. Li X, Zhang LM (2009) Characterization of dual-structure pore-size distribution of soil. Can Geotech J 46(2):129–141

25. Liu K, Chen WB, Feng WQ, Yin JH (2018) Experimental study on the unsaturated behaviour of a compacted soil. In: 7th international conference on unsaturated soils (UNSAT2018), 3rd–5th August 2018, The Hong Kong University of Science and Technology (HKUST), Hong Kong, China

26. Liu H, Li PF, Zhang ZY (2005) Prediction of the post-construction settlement of the high embankment of Jiuzhai-Huang-long airport. Chin J of Geotech Eng 27(1):90–93 **(in Chinese)**

27. Maatouk A, Leroueil S, La Rochelle P (1995) Yielding and critical state of a collapsible unsaturated silty soil. Géotechnique 45(3):465–477

28. Ng CW, Chiu AC (2001) Behavior of a loosely compacted unsaturated volcanic soil. J Geotech Geoenviron Eng ASCE 127(12):1027–1036

29. Rampino C, Mancuso C, Vinale F (2000) Experimental behaviour and modelling of an unsaturated compacted soil. Can Geotech J 37(4):748–763

30. Salim W, Indraratna B (2004) A new elastoplastic constitutive model for coarse granular aggregates incorporating particle breakage. Can Geotech J 41(4):657–671

31. Satija BS, Gulhati SK (1979) Strain rate for shearing testing of unsaturated soil. In: Proceedings of the sixth Asian regional conference on soil mechanics and foundation engineering, Singapore, pp 83–86

32. Schofield A, Wroth P (1968) Critical state soil mechanics. McGraw-Hill, London

33. Seif El Dine B, Dupla JC, Frank R, Canou J, Kazan Y (2010) Mechanical characterization of matrix coarse-grained soils with a large-sized triaxial device. Can Geotech J 47(4):425–438

34. Shelley TL, Daniel DE (1993) Effect of gravel on hydraulic conductivity of compacted soil liners. J Geotech Eng 119(1):54–68

35. Shi XS, Herle I (2017) Numerical simulation of lumpy soils using a hypoplastic model. Acta Geotech 12(2):349–363

36. Shi XS, Herle I, Muir Wood D (2018) A consolidation model for lumpy composite soils in open-pit mining. Géotechnique 68(3):189–204

37. Shi XS, Nie J, Zhao JD, Gao Y (2020) A homogenization equation for the small strain stiffness of gap-graded granular materials. Comput Geotech 121:103440

38. Shi XS, Yin J (2018) Estimation of hydraulic conductivity of saturated sand-marine clay mixtures with a homogenization approach. Int J Geomech 18(7):04018082

39. Shi XS, Zhao JD (2020) Practical estimation of compression behavior of clayey/silty sands using equivalent void-ratio concept. J Geotech Geoenviron Eng 146(6):04020046

40. Shi XS, Zhao J, Yin J, Yu Z (2019) An elastoplastic model for gap-graded soils based on homogenization theory. Int J Solids Struct 163:1–14

41. Sivakumar V (1993) A critical state framework for unsaturated soil. Ph.D. Dissertation, University of Sheffield, Sheffield, UK

42. Sivakumar V, Sivakumar R, Boyd J, Mackinnon P (2010) Mechanical behaviour of unsaturated kaolin (with isotropic and anisotropic stress history). Part 2: performance under shear loading. Géotechnique 60(8):595–609

43. Tarantino A, Romero E, Cui YJ (eds) (2009) Laboratory and field testing of unsaturated soils. Springer, Amsterdam, p 220

44. Tarantino A, Gallipoli D, Augarde CE et al (2011) Benchmark of experimental techniques for measuring and controlling suction. Géotechnique 61(4):303–312

45. Thomas SD (1987) The consolidation behavior of gassy soils. Ph.D. Dissertation, University of Oxford, Oxford, UK

46. Toll DG (1990) A framework for unsaturated soil behavior. Géotechnique 40(1):31–44

47. Toll DG, Ong BH (2003) Critical-state parameters for an unsaturated residual sandy clay. Géotechnique 53(1):93–103

48. Vanapalli SK, Fredlund DG, Pufahl DE, Clifton AW (1996) Model for the prediction of shear strength with respect to soil suction. Can Geotech J 33(3):379–392

49. van Genuchten MT (1980) A closed-form equation for predicting the hydraulic conductivity of unsaturated soils. Soil Sci Soc Am J 44(5):892–898

50. Wang HL, Cui YJ, Lamas-Lopez F et al (2017) Effects of inclusion contents on resilient modulus and damping ratio of unsaturated track-bed materials. Can Geotech J 54:1672–1681

51. Wang HL, Cui YJ, Lamas-Lopez F et al (2018) Permanent deformation of track-bed materials at various inclusion contents under large number of loading cycles. J Geotech Geoenviron Eng ASCE 144(8):04018044

52. Wang HL, Cui YJ, Lamas-Lopez F et al (2018) Investigation on the mechanical behavior of track-bed materials at various contents of coarse grains. Constr Build Mater 164:228–237

53. Wang Q, Pufahl DE, Fredlund DG (2002) A study of critical state on an unsaturated silty soil. Can Geotech J 39(1):213–218

54. Wheeler SJ, Sharma RS, Buisson MSR (2003) Coupling of hydraulic hysteresis and stress–strain behaviour in unsaturated soils. Géotechnique 53(1):41–54

55. Wheeler SJ, Sivakumar V (1993) Development and application of a critical state model for unsaturated soil. In: Predictive soil mechanics. Proceedings of the Wroth memorial symposium, Oxford, 1992

56. Wheeler SJ, Sivakumar V (1995) An elasto-plastic critical state framework for unsaturated soil. Géotechnique 45(1):35–53

57. Xiao Y, Coop MR, Liu H, Liu HL, Jiang JS (2016) Transitional behaviors in well-graded coarse granular soils. J Geotech Geoenviron Eng ASCE 142(12):06016018

58. Yan Y, Cui YF, Guo J et al (2020) Landslide reconstruction using seismic signal characteristics and numerical simulations: Case study of the 2017 "6.24" Xinmo landslide. Eng Geol 270:105582

59. Yao YP, Niu L, Cui WJ (2014) Unified hardening (UH) model for overconsolidated unsaturated soils. Can Geotech J 51(7):810–821

60. Yao YP, Liu L, Luo T (2018) A constitutive model for granular soils. Sci China Technol Sc 61(10):1546–1555

61. Yin JH (2003) A double cell triaxial system for continuous measurement of volume changes of an unsaturated or saturated soil specimen in triaxial testing. Geotech Test J 26(3):353–358

62. Yin ZY, Hicher PY, Dano C, Jin YF (2016) Modeling mechanical behavior of very coarse granular materials. J Eng Mech ASCE 143(1):C4016006

63. Zhan LT (2003) Field and laboratory study of an unsaturated expansive soil associated with rain-induced slope stability. Ph.D. Dissertation. The Hong Kong University of Science and Technology, Hong Kong, China

64. Zhang LL, Fredlund DG, Zhang LM, Tang WH (2004) Numerical study of soil conditions under which matric suction can be maintained. Can Geotech J 41(4):569–582

65. Zhang LM, Li X (2010) Microporosity structure of coarse granular soils. J Geotech Geoenviron Eng ASCE 136(10):1425–1436

66. Zhao HF, Zhang LM, Chang DS (2013) Behavior of coarse widely graded soils under low confining pressures. J Geotech Geoenviron Eng ASCE 139(1):35–48

67. Zhao HF, Zhang LM (2014) Effect of coarse content on shear behavior of unsaturated coarse granular soils. Can Geotech J 51(12):1371–1383

68. Zhou C (2014) Experimental study and constitutive modelling of cyclic behaviour at small strains of unsaturated silt at various temperatures. Ph.D. Dissertation, The Hong Kong University of Science and Technology, Hong Kong, China

69. Zhou C, Ng CWW (2015) Simulating the cyclic behaviour of unsaturated soil at various temperatures using a bounding surface model. Géotechnique 66(4):344–350

70. Zhou C, Ng CWW, Chen R (2015) A bounding surface plasticity model for unsaturated soil at small strains. Int J Numer Anal Methods Geomech 39(11):1141–1164

71. Zhou C, Ng CWW (2016) Simulating the cyclic behaviour of unsaturated soil at various temperatures using a bounding surface model. Géotechnique 66(4):344–350